STUK

Groundwater flow analysis and dose rate estimates from releases to wells at a coastal site

Eero Kattilakoski, Vesa Suolanen
VTT Energy

In STUK this study was supervised by **Esko Ruokola**

ABSTRACT

In the groundwater flow modelling part of this work the effective dilution volume in the well scenario was estimated by means of transient simulations of groundwater flow and transport, which are coupled due to the varying salinity. Both deep, drilled wells and shallow surface wells in the vicinity of the repository were considered. The simulations covered the time period from the present to 1000 years after the present.

Conceptually the fractured bedrock consists of planar fracture zones (with a high fracture density and a greater ability to conduct water) and the intact rock (in which the fracture density and the hydraulic conductivity are low). For them the equivalent-continuum model was applied separately. Thus, the fractured bedrock was considered as piecewise homogeneous (except for the depth dependence) and isotropic continuum with representative average characteristics.

A generic simulation model for groundwater flow and solute transport was developed on the basis of geological, hydrogeological and hydrogeochemical data at a coastal area. The simulation model contains all the data necessary for the numerical simulations, i.e. the groundwater table and topography, salinity, the postglacial land uplift and sea level rise, the conceptual geometry of fracture zones, the hydraulic properties of the bedrock as well as the description of the modelling volume. The model comprises an area of about 26 km². It covers an island and the surrounding sea.

The finite element code FEFTRA (formerly known as FEFLOW) was used in this work for the numerical solution.

The channelling along the flow routes was found to be critical for the resulting in a well. A deep well may extend near the area of the deep flow routes, but in order to get flow routes into a shallow well, it has to be placed in the immediate vicinity of the discharge areas.

According to the groundwater flow analyses the effective dilution volume of the well seems to vary from 30 000 m³/a to 460 000 m³/a. Due to the placing of the shallow wells in the discharge areas, the dilution calculated in the shallow well was shown to be close to that calculated in the deep well. In conservative considerations the value around 90 000 m³/a can be regarded as a representative expectation value of the effective dilution of the well. This dilution volume value was also suggested by the most realistic modelling approach of the groundwater flow analysis. It was used as basis when calculating the nuclide specific dose conversion factors (DCF's) for the drinking water pathway. The DCF's were calculated for unit release rates (1 Bq/a) and the assumed water consumption rate was 2 litres/day.

CONTENTS

1 INTRODUCTION

1.1 Groundwater flow modelling

In recent safety analyses the effective dilution volumes assumed for the well scenarios vary considerably (e.g., 100 000 m³/a in the Finnish TILA-99 and 2 630 m³/a in the Swedish SR-97) (Vieno & Nordman, 1999; SKB, 1999). In those analyses, the choice of the dilution volumes is not based on a computational estimation of the groundwater flow. An estimate of the dilution volume as result of a careful analysis should be based on a realistic description of the structures and the hydraulic conductivity of the bedrock. Also, as regards to the placing and the depth of the wells several alternatives should be considered.

In this work the effective dilution volume in the well scenario is estimated by means of the simulations of groundwater flow and transport, which are coupled due to the varying salinity. Two of the selected approaches utilise flow route calculations, whereas the third involves tracer transport calculations using the simulated pressure and salinity fields. The task is performed by applying a model based on the porous medium concept and the finite element method. Both deep, drilled wells and shallow surface wells in the vicinity of the repository are considered.

1.2 Dose rate estimates

In the study nuclide specific dose rates, arising from consumption of water from a well, are calculated based on unit release rates (Bq/a) into the rock volume affected by the well and on the estimated effective dilution volume of the well. Also, the dose responses in biosphere brought about by the drinking water pathway are considered by using the estimated release rates of the base scenario of the recent spent fuel disposal safety assessment (TILA-99).

2 MODELLING APPROACH

2.1 Physical background and basic assumptions

The varying density of groundwater and the post-glacial land uplift and sea level rise are taken into account in the numerical simulations of coupled and transient groundwater flow and solute transport. The simulations cover the time period from the present to 1000 years after the present.

In this work the equivalent-continuum approach (EC), where the fractured bedrock is considered as a continuum, is used. It is assumed that in a subvolume of the bedrock the hydraulic characteristics can be averaged so that this EC representation as a whole behaves similarly as the actual rock with regard to groundwater flow and mass transport. Conceptually the fractured bedrock consists of planar fracture zones (with a high fracture density and a greater ability to conduct water) and the intact rock (in which the fracture density and the hydraulic conductivity are low). For them the equivalent-continuum model is applied separately. Thus, the fractured bedrock is considered as piecewise homogeneous (except for the depth dependence) and isotropic continuum with representative average characteristics.

The EC method is quite approximate, because the determination of the average hydraulic properties is often difficult due to the scarce field data with wide range and constitutes a major source of uncertainty in the simulations. Moreover, the results obtained with the EC model represent average values over large volumes of the bedrock.

The repository and the surrounding disturbed zone of the bedrock are modelled as a planar structure. The transmissivity of the repository in the model represents the situation that the hydraulic conductivity of the repository region is orders of magnitude higher than that of the surrounding intact rock. The effects of the construc-

tion and the operation phase are not considered. Therefore, the repository is assumed to be closed and fully saturated at the beginning of the simulation period. Also, the effects of the temperature changes caused by the heat generation of the spent nuclear fuel are not considered.

The modelled bedrock volume is assumed to be fully saturated. In the cases of the drilled wells the modelled volume is assumed to lie below the layer of soil and the surface part of the bedrock. These top layers possess high hydraulic conductivities. The uppermost layer of the bedrock is relatively transmissive due to its intensive fracturing.

Residual pressure based on the elevation of the groundwater table is used as surface boundary condition. It is used also in the cases of the shallow wells, which do not extend to the bedrock. In these cases the topmost layers of the model describe the soil. The hydraulic conductivity of the soil is adjusted to allow an adequate portion of water to infiltrate into the modelled volume. In Finland, under the present natural conditions, about half of the precipitated water is transferred back to the atmosphere by evaporation and transpiration. A major part of the rest moves on as surface runoff or subsurface flow in the soil (Anon., 1986). Only a small portion of the precipitated water infiltrates into the bedrock.

2.2 Mathematical model

The mathematical formulation of groundwater flow and mass transport in the equivalent continuum (EC) approach comprises two coupled and non-linear partial differential equations. One of them describes the flow of water with variable density under the influence of the pressure field. The other equation describes the amount of mass transported with the flowing water. The equations are based on the law of conservation of mass. They

are presented below in reduced forms (e.g., without the terms representing sinks and sources), as they are applied in this study. A more general formulation of the equations is given by, e.g., Huyakorn & Pinder (1983) and Löfman & Taivassalo (1993).

The flow equation for a steady state can be expressed in terms of the residual pressure p_r (Pa)—the total pressure minus the hydrostatic component of freshwater (Bear, 1979; Huyakorn & Pinder, 1983; de Marsily, 1986):

$$\nabla \cdot (\frac{\rho \boldsymbol{k}}{\mu}(\nabla p_r + (\rho - \rho_0)g\nabla z)) = 0 , \tag{1}$$

where

ρ is the density of water (kgm^{-3}),

ρ_0 is the freshwater density (kgm^{-3}),

μ is the dynamic viscosity of water (kgm^{-1}s^{-1}),

$\boldsymbol{k}$ is the permeability tensor of the medium (m^2),

g is the gravitational acceleration (=9.81 ms^{-2}) and

z is the elevation relative to the sea level (m).

The flow equation (1) is written in the steady state form, because in this work the temporal variations of the amount of water in the bedrock are assumed to follow solely from the changes in the boundary conditions. The behaviour of the average flow and the corresponding boundary conditions are changing sufficiently slowly over periods of several years, so the flow can be taken to be always in steady state.

The permeability tensor $\boldsymbol{k}$ in Eq. (1) can be expressed in terms of the hydraulic conductivity $\boldsymbol{K}$ (m/s):

$$\boldsymbol{k} = \frac{\boldsymbol{K}\mu}{\rho g} . \tag{2}$$

The dependence of the density of water on the salinity S (kg/m^3; TDS) is approximated linearly as

$$\rho = \rho_0 + a_C S , \tag{3}$$

where a_C is the coefficient of the density dependence on the salinity (–). The dependence of the density of water on the pressure is ignored, since the compressibility of water is assumed to be insignificant.

Assuming that the transport of solutes through the homogeneous, isotropic and porous medium is governed by the phenomena of convection, dispersion and molecular diffusion, the equation describing the mass transport can be written in terms of the concentration of the solute (kg/m^3) as follows (Bear, 1979; Huyakorn & Pinder, 1983; de Marsily, 1986):

$$\nabla \cdot (\boldsymbol{D}\nabla c) - \nabla \cdot (\boldsymbol{q}c) = \phi_f \frac{\partial c}{\partial t} , \tag{4}$$

where

$\boldsymbol{D}$ is the hydrodynamic dispersion tensor (m^{2}s^{-1}),

$\boldsymbol{q}$ is the Darcy velocity (ms^{-1}) and

ϕ_f is the flow porosity (–).

The first term in the left-hand side of Equation (4) represents the change in the dispersive and diffusive mass flux of solutes, whereas the second term characterises the convective mass flux. The right-hand side describes the temporal change in the mass of solutes.

The components of the hydrodynamic dispersion tensor $\boldsymbol{D}$ in Eq. (4) are (Bear, 1979)

$$D_{ij} = \varepsilon_T |\boldsymbol{q}| \delta_{ij} + (\varepsilon_L - \varepsilon_T)\frac{q_i q_j}{|\boldsymbol{q}|} + \phi_d D_0, \qquad i, j = 1, 2, 3, \tag{5}$$

where

ε_L is the longitudinal dispersion length (m),

ε_T is the transversal dispersion length (m),

δ_{ij} is the Kronecker delta function (–),

ϕ_d is the diffusion porosity (–) and

D_0 is the molecular diffusion coefficient in water (m^2 s^{-1}).

The Darcy velocity $\boldsymbol{q}$ in Eqs. (4) and (5) in terms of the residual pressure p_r is

$$\boldsymbol{q} = -\frac{\boldsymbol{k}}{\mu}(\nabla p_r + (\rho - \rho_0)g\nabla z) . \tag{6}$$

Assuming a parallel fracture idealisation, in which the bedrock consists of equally spaced and parallel fractures separated by matrix blocks, the flow porosity ϕ_f in Equation (4) can be defined as the volume of fractures per unit volume of the entire system:

$$\phi_f = \frac{b}{a + b} , \tag{7}$$

where a is half the matrix block thickness (m) and b is half the fracture aperture (m). The (volume) fracture aperture $2b$ (m) is expressed as a function of the fracture spacing $2a$ and the hydraulic con-

ductivity $\boldsymbol{K}$ as follows (Taivassalo & Saarenheimo, 1991; Vieno et al., 1992):

$$2b = C_{vh}(\frac{12\mu}{\rho_0 g}\boldsymbol{K}2a)^{\frac{1}{3}}, \tag{8}$$

where C_{vh} is the coefficient for the dependence between the volume and hydraulic fracture aperture (–).

2.3 Numerical solution method

The flow equation (1) and the transport equation (4) are coupled by the density ρ and the Darcy velocity $\boldsymbol{q}$ (Eq. (6)). This results in a system of two non-linear partial differential equations that can rarely be solved analytically. The finite element code FEFTRA (formerly known as FEFLOW) was used in this work for the numerical solution (Taivassalo et al., 1991; Löfman & Taivassalo, 1993; Laitinen, 1995; FEFTRA, 1999).

The finite element method with linear elements was employed. The conventional Galerkin technique was applied to the flow equation (1). In order to avoid the numerical problems related to highly convective cases the transport equation (4) was solved using the streamline-upwind/Petrov-Galerkin (SUPG) method (Brooks and Hughes, 1992; implemented in FEFTRA by Laitinen, 1995).

In the coupled cases non-linearities were treat-ed by the Picard iteration scheme (Huyakorn and Pinder, 1983), in which, for each time step, the flow and the transport equation are solved sequentially until the convergence is attained. At the end of each iteration sweep the concentration values were updated using an underrelaxation scheme. This way the oscillations of concentration changes from iteration to iteration are reduced.

An initial estimate for the nodal values of the residual pressure and the concentration at the beginning of the first iteration sweep of each time step was obtained by using a linear time extrapolation formula. The mass matrices resulting from the finite element formulation were formed by a diagonalization procedure known as "lumping" (Huyakorn and Pinder, 1983). In practical problems this leads to a more stable solution than with a "consistent" matrix.

In the coupled calculations the conjugate-gradient method was used to solve the finite element formulation of Equation (1) for residual pressure and the Gauss-Seidel method to solve the finite element formulation of Equation (4) for concentration.

In one of the approaches used in this work the transport equation (4) for a tracer was solved using the previously simulated residual pressure and salinity fields. The Gauss-Seidel method was used to solve the matrix equation (4) in these cases (Laitinen, 1994).

3 FLOW AND TRANSPORT MODEL

3.1 Modelling volume

A generic simulation model for groundwater flow and solute transport is developed on the basis of geological, hydrogeological and hydrogeochemical data at a coastal area. The simulation model contains all the data necessary for the numerical simulations, i.e. the groundwater table and topography, salinity, the postglacial land uplift and sea level rise, the conceptual geometry of fracture zones, the hydraulic properties of the bedrock as well as the description of the modelling volume.

The model comprises an area of about 26 km². It covers an island and the surrounding sea. The depth of the modelled domain is 1.5 km, due to the exponentially decreasing hydraulic conductivity of the intact rock and the transmissivity of the fracture zones (the flow deeper in the bedrock can be considered insignificant). The distance of the boundaries from the centre of the island is about 2–3 km. Thus, the locations of the vertical and bottom boundaries can be assumed to be far enough from the repository area to make the effects of the uncertainty associated with the boundary conditions insignificant.

3.2 Geometry of fracture zones

The modelled volume has been divided into hydraulic units, the intact rock and the fracture zones. The geometry of the fracture zones (Fig. 1) contains 31 individual zones. They are modelled
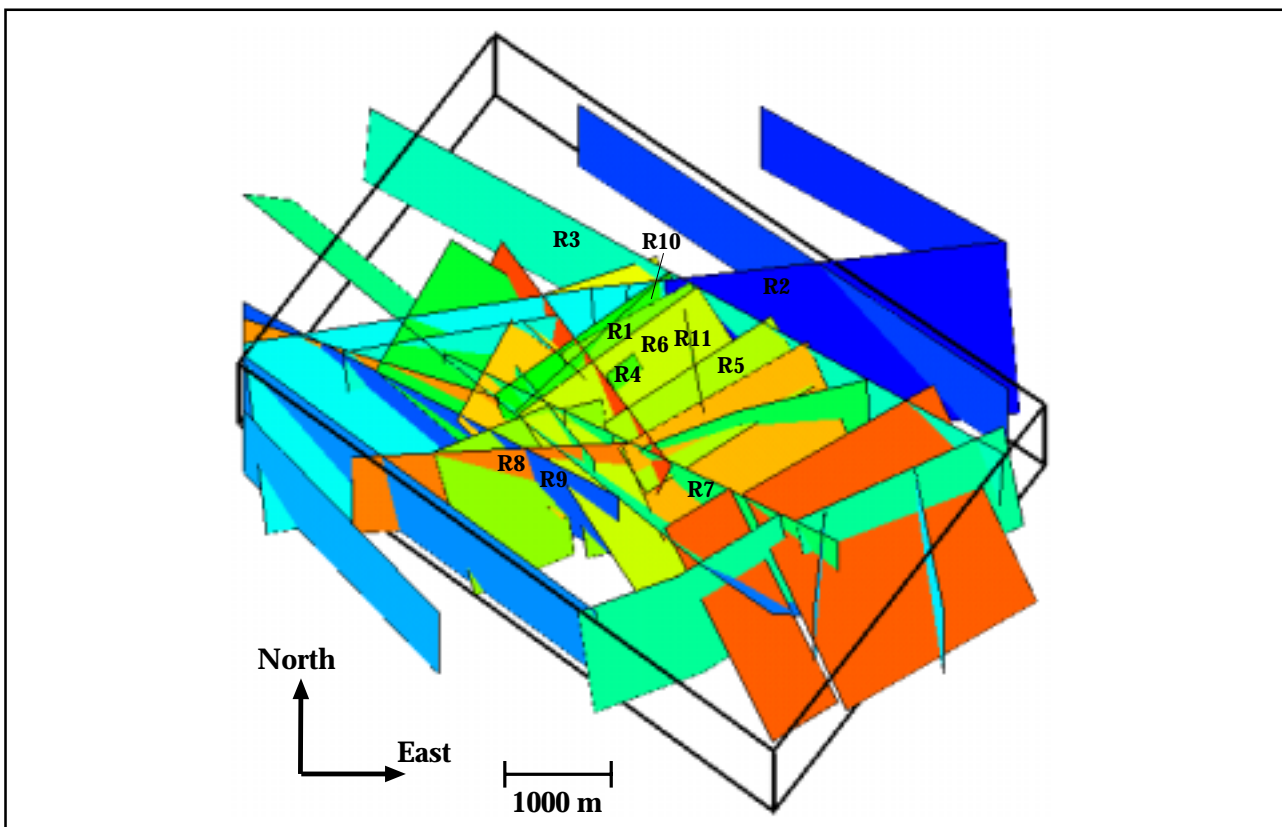

Figure 1. *Conceptual fracture zone geometry for the site. The modelled volume is outlined.*

explicitly resulting in a relatively complex geometry. Most of the zones extend to the bottom of the model. All the zones are assumed to be of uniform thickness of 10 metres. The zone density is the largest at the centre of the island, because the field investigations have been focused there.

3.3 Repository and surrounding disturbed zone

The repository and the surrounding disturbed zone is located at the depth of 500 metres and intersected by two fracture zones, R10 and R11. The thickness of the repository is assumed to be 5 metres. The principles for the construction of the layout are given in the work by Riekkola et al. (1996).

3.4 Finite element mesh

For the numerical simulations the modelled volume is discretised into a finite element mesh. The base mesh consisting of only three-dimensional linear hexahedral elements representing the intact rock is created first. Each of the topmost three element layers is 5 metres thick to assure a proper setting of the hydraulic conductivity of the soil. From the depth of 15 metres the size of the elements increases towards the bottom in the vertical direction from about 17 metres to about 220 metres at the bottom. The thickness of the element layer just below the depth of 500 metres is 100 metres. In the horizontal direction the discretisation is the densest at the centre of the island. The average size of the top face of the three-dimensional elements is about 70×70 m² there.

Due to the planar form of a structure and the high contrast of its hydraulic conductivity with the hydraulic conductivity of the rock between the structures (more than two orders of magnitude), water in the zones can be assumed to flow parallel to the plane of the zone enabling the use of two-dimensional elements. Thus, the base mesh is modified to correspond to the geometry of the fracture zones (Fig. 1) by adding two-dimensional quadrangular and triangular elements for the fracture zones. Because the two-dimensional elements do not have physical thickness, the thickness of the fracture zones is taken care of mathe-

matically (e.g., the thickness in the flow equation is included in the transmissivity).

The final finite element mesh employed in the simulations contains 54 432 three-dimensional hexahedral elements and 20 211 two-dimensional quadrangular and triangular elements (Fig. 2). The plane representing the repository consists of 151 two-dimensional quadrangular elements of size about 70×70 m².

3.5 Properties of bedrock and water

Numerical simulations are based on the mathematical model presented in Section 2.2. The governing equations for flow and transport include several properties of bedrock and water, which are needed as input parameters in the simulations.

Transmissivity of the fracture zones and the repository

The transmissivity of the fracture zones T (m²/s) is assumed to vary exponentially as follows (Saksa et al., 1996):

$$T = T_0 \cdot 10^{f(d)}, \tag{9}$$

where T_0 (m²/s) is the transmissivity on the surface, d (m) is the depth relative to the sea level and

$$f(d) = -7 \cdot 10^{-10} d^3 + 3 \cdot 10^{-6} d^2 - 5 \cdot 10^{-3} d. \tag{10}$$

The fracture zones are divided in two categories according to the transmissivity. The classification of the fracture zones is shown in Table I.

The repository plate is assumed to have an isotropic transmissivity $5 \cdot 10^{-8}$ m²/s, which was applied in the base case by Vieno et al. (1992). This value includes the hydrological properties of the tunnel system and the surrounding disturbed rock zone. It represents the situation, where the hydraulic conductivity of the sand-bentonite backfill of the tunnel (area about 15 m²) is $5 \cdot 10^{-9}$ m/s (Pusch, 1990) and that of the disturbed rock zone (area about 20 m²) $5 \cdot 10^{-8}$ m/s. This value is nearly three orders of magnitude higher than in the surrounding intact rock at the depth of 500 metres.

Table I. *The transmissivity of the fracture zones T_0 (m²/s), the hydraulic conductivity K_0 (m/s) of the intact rock and the fracture spacing $2a_0$ (m) on the surface of the model. The thickness of the zones is 10 m. The transmissivity T and the hydraulic conductivity K at the depth of 500 m are also shown.*

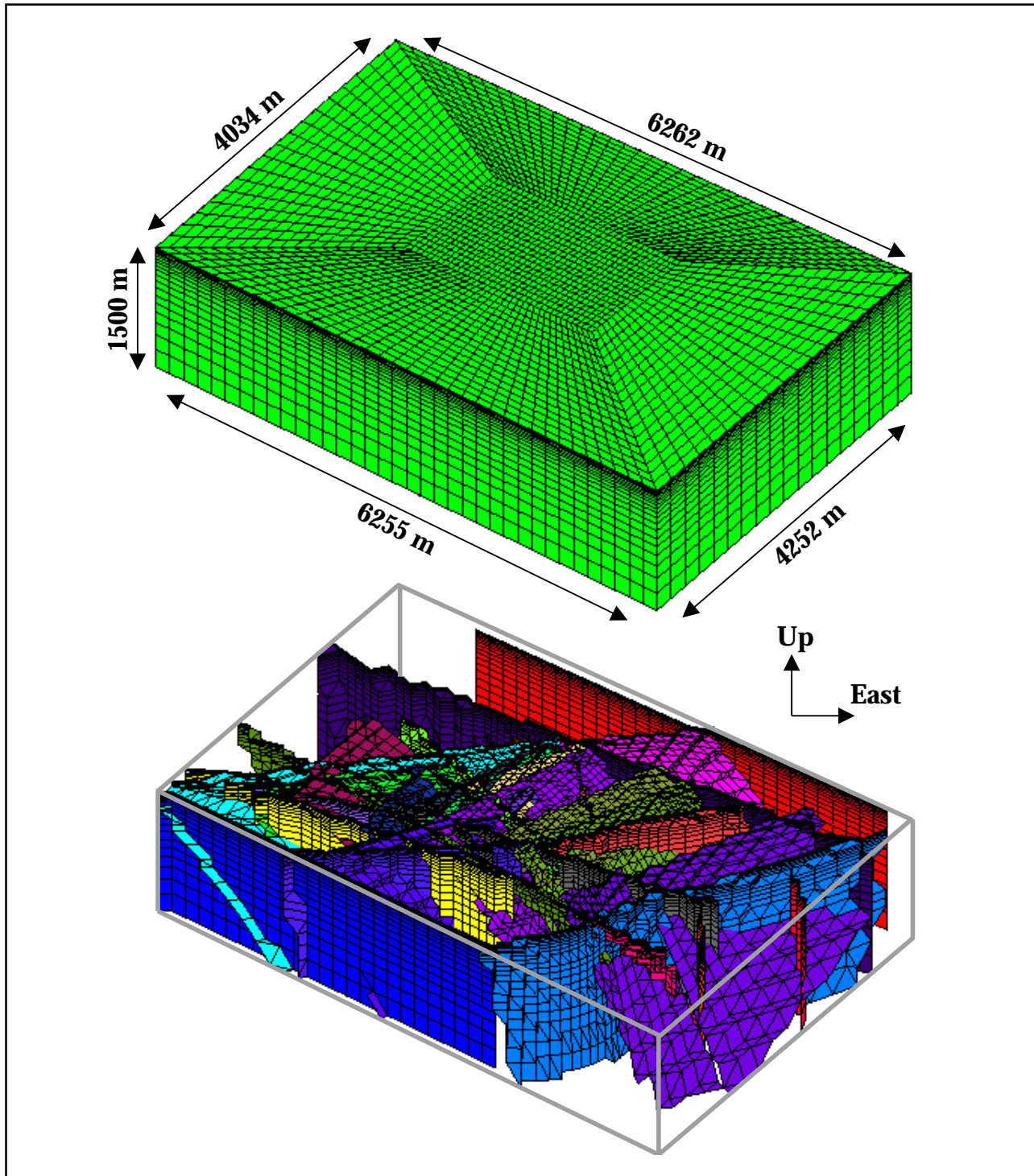| Class	T_0 or K_0	T or K (depth 500 m)	$2a_0$	Labelled zones
A	$4.4 \cdot 10^{-4}$	$6.4 \cdot 10^{-6}$	0.07	R2, R3, R5, R6, R7, R8, R9
B	$1.0 \cdot 10^{-5}$	$1.5 \cdot 10^{-7}$	0.07	R1, R4, R10, R11
Intact rock	$5.0 \cdot 10^{-9}$	$7.3 \cdot 10^{-11}$	0.15	—

Figure 2. *Finite element mesh. The three-dimensional elements (54 432) represent the rock between the fracture zones (top) and the two-dimensional elements (20 211) the fracture zones (bottom).*

Table II. *Properties of the bedrock and water employed in the simulations.*

Symbol	Parameter	Equation	Value
ρ_0	Freshwater density	1, 3, 6, 8	998.585 kg m^{-3}
a_c	Density dependence on TDS concentration (salinity)	3, 17	0.71
ε_L	Longitudinal dispersion length	5	200 m
ε_T	Transversal dispersion length	5	50 m
C_{vh}	Coefficient for dependence between volume and hydraulic aperture	8	10
μ	Viscosity of water	1, 2, 6, 8	$1.0 \cdot 10^{-3}$ kg m^{-1}s^{-1}
ϕ_d	Diffusion porosity	5	$1.0 \cdot 10^{-3}$
D_0	Molecular diffusion coefficient in water	5	$1.0 \cdot 10^{-9}$ m^2 s^{-1}

Hydraulic conductivity of the intact rock

The intact rock is modelled conceptually as a homogeneous (equivalent) continuum with representative average characteristics, i.e. the small-scale hydraulic conductivities are averaged. The conductivities thus obtained represent the similar overall behaviour of the network of fractures on a larger length scale. The hydraulic conductivity used in the simulations is the upscaled effective average conductivity, which is required due to the selected modelling approach. The hydraulic conductivity in this study is given by

$$K = K_0 \cdot 10^{f(d)}, \tag{11}$$

where K_0 (m/s) is the hydraulic conductivity on the surface, d (m) is the depth relative to the sea level and $f(d)$ is given by Equation (10).

Flow porosity

The experimental data for the flow porosity in the transport equation (4) is usually rarely available. In reality the flow porosity is not constant, but it varies and is related to the other varying properties of the rock (e.g., the hydraulic conductivity). In this study the flow porosity (Eqs. (7) and (8)) is computed from the spacing *2a* of the fractures with flowing water and the transmissivity *T* of the fracture zone (Equation (9)) or the hydraulic conductivity *K* (Equation (11)) (Vieno et al., 1992; Taivassalo & Saarenheimo, 1991).

An assumption is made on the depth dependence of the spacing of the water-bearing fractures:

$$2a = 2a_0 \cdot 2^{-\frac{z}{500}}, \tag{12}$$

where $2a_0$ (m) is the fracture spacing at the surface. The approximation (12), which states that the spacing doubles within each 500 metres, is applied for both the fracture zones and the intact rock. The surface values for the intact rock are selected so that the resulting flow porosity is in line with the values reported in the literature for the crystalline rock. The fracture spacing at the surface for the fracture zones and the intact rock is shown in Table I.

Miscellaneous

Values used for the other properties are shown in Table II. The freshwater density and the coefficient of the density dependence on salinity are based on the correlation of the measured density and salinity (e.g., Lampén & Snellman, 1993). The viscosity of water is a well known parameter (Lide, 1990).

Based on studies by Vieno et al. (1992) and Taivassalo & Saarenheimo (1991) a constant value (10) is used for the dependence between the volume and the hydraulic fracture aperture C_{vh}.

The common assumption is that the longitudinal dispersion length is about 10 % of the length of a transport route (e.g., de Marsily, 1986). The value used (Table II) is a compromise between the values for long transport routes and the size of the elements in the model. Additionally, the longitudinal dispersion length is selected to be large enough to avoid numerical problems associated to too large Peclet numbers. On the other hand, the dispersion in the model increases uncertainty in the transport-based modelling approach (see Section 4.2.3). The transversal dispersion length is

assumed to be 25 % of the longitudinal dispersion length.

3.6 Postglacial land uplift and global sea level rise

Pàsse (1996) has constructed a mathematical model for both the land uplift and the global sea level rise in the area covered by the Scandinavian ice during the Weicselian glaciation. Instead of the commonly employed exponential functions, he used *arctan*-functions, which gave more consistent behaviour of the land uplift and the sea level changes before a period covered by the empirical data. In this work the glacio-isostatic land uplift U (m) is described by the function

$$U(t) = -0.6366 \cdot 245 \cdot$$
$$(\arctan(\frac{12500}{9500}) - \arctan(\frac{12500+t}{9500})) \cdot \qquad (13)$$

The glacio-eustatic sea level rise E (m) is written as

$$E(t) = -0.6366 \cdot 50 \cdot$$
$$(\arctan(\frac{9350}{1375}) - \arctan(\frac{9350+t}{1375})) \cdot \qquad (14)$$

Thus, the net land uplift U_{net} (m) relative to the sea level is obtained as

$$U_{net}(t) = U(t) - E(t) . \qquad (15)$$

According to the function (15) the land will still rise about 40 metres during the next 10 000 years.

3.7 Initial and boundary conditions

Salinity

Initially the following, only depth dependent salinity model is employed (Löfman, 1999):

$$S_0(z) = \begin{cases} -0.04982z, & 0 \leq z \leq -100 \\ 3.582e^{-0.0033z}, & -100 \leq z \leq -900 \\ 72.0, & -900 \leq z \leq -1500. \end{cases} \qquad (16)$$

The linear model is used from the surface to the depth of 100 metres. From 100 metres to 900 met-

res the exponential model is applied, whereas a constant value 72 g/l is used from the depth of 900 metres to the bottom of the model.

At the surface of the model a zero salinity (0 g/l) is used for the area, which at each time represents the groundwater table, due to the freshwater flow into the modelled volume. Salinity 5 g/l is applied for the Baltic Sea and for the lakes developed from the local topographical depressions. On the vertical edges and at the bottom time-dependent fixed salinity is used as in the case of the pressure boundary condition described below.

Pressure

Residual pressure based on the elevation of the groundwater table is used as an initial and boundary condition on the surface of the modelled volume (Fig. 3). In the future the area of the island will enlarge due to the net effect of the postglacial land uplift and the global sea level rise (Eqs. (13) – (15)). Thus, the groundwater table will rise. The net uplift of the groundwater table is defined to be 0.56 times the net land uplift given by Equation (15).

In the rest of the modelled volume the initial pressure is assumed to be hydrostatic. The values assigned to the nodes are calculated as follows:

$$p_r = -a_C g \int_0^z S_0(z) dz , \qquad (17)$$

where a_C is the density dependence on the salinity (0.71, see Table II), g is the gravitational acceleration (9.81 m/s²) and $S_0(z)$ is the salinity given in Equation (16).

On the vertical faces time-dependent residual pressures are used. The current value for each boundary node on the vertical faces is the pressure in the nearest interior node from the previous time step. Thus, the amount of water flowing through the vertical boundaries is approximated from the previous results.

This method of using the result of the previous time step provides a convenient way to use specified nodal values as boundary conditions in the transient simulations. However, the finite resolution of the boundary elements and the time steps together with the velocity of water results in under- or overestimation of the amount of water flowing through the vertical faces of the modelled

volume. If the time that it takes from water to move through the boundary element is shorter than the current time step, the boundary condition retards the flow near the boundary. On the contrary, the flow is strengthened by the boundary condition, if water actually flows slower in the boundary element.

At the bottom of the model the no-flow boundary condition is applied. Due to the linearly decreasing hydraulic conductivities the amount of water flowing deeper in the bedrock can be considered insignificant.

Especially near the places, where highly transmissive fracture zones reach the ground surface, the selection of the groundwater table may lead to unrealistically high fluxes of water into the mod-
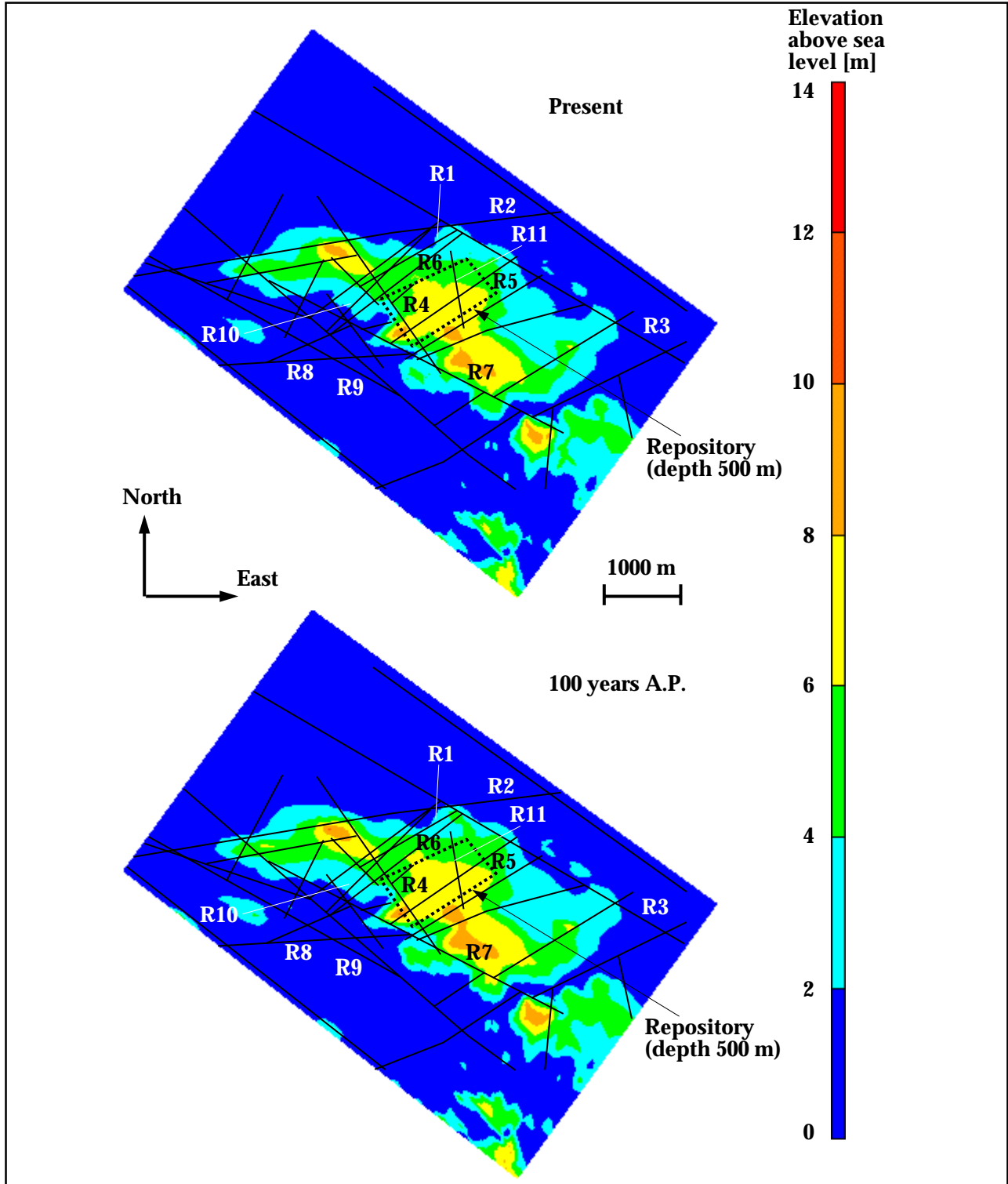

Figure 3a. *Surface boundary condition of the model at present and at 100 years after the present (A.P.).*

elled domain. In such regions the groundwater table would be expected to be lower than in the regions away from the zones. The computed total infiltration rate into the modelled domain is approximately 42 mm/a, which is about 7.6 % of the assumed average precipitation 550 mm/a. Thus, the computed value may be somewhat large, which suggests too high transmissivities in some fracture zones. The infiltration rate was computed at the depth of 2.5 metres, which is the centre of the uppermost element layer.

3.8 Wells

The dilution was calculated for six water wells (Fig. 4). They were located in the vicinity of the discharge areas or in the intermediate region. Siting of the drilled wells was chosen so that the salinity does not increase very high in the bottom parts of the wells.

Three of the examined wells are drilled wells. They are modelled by giving a residual pressure boundary condition p_r=0 Pa in the nodes depicting the well. The wells are placed in the model at 100 years after the present (A.P.).

The drilled well #1 is located some hundred metres south-west from the northern discharge area at 100 years A.P. (SA2 in Fig. 4). It is 223 metres deep and intersects the fracture zone R1 in the topmost part of the zone and R2 deep in the bedrock (77–138 m).

The drilled well #2 is sited above the repository between the surface traces of the fracture zones R4 and R5. It is 177 metres deep and intersects the south-east dipping fracture zones R4 and R6 at the depth of 177 m.

The well #3 is drilled about 500 metres east from the southern discharge area at 100 years A.P. (SA1 in Fig. 4). In the first simulation this well was taken as deep as the northest drilled well (223 m), but the simulation depth was decreased due to the too high capacity (about 59 000 m³/a at 100 years A.P. and about 131 000 m³/a at 1000 years A.P.) obtained as the result of the first simulation. The capacity of the 15 metres deep well finally simulated is somewhat smaller than that of the well #1 (Table III). The well #3 intersects the fracture zone R7 in the topmost part of the zone.
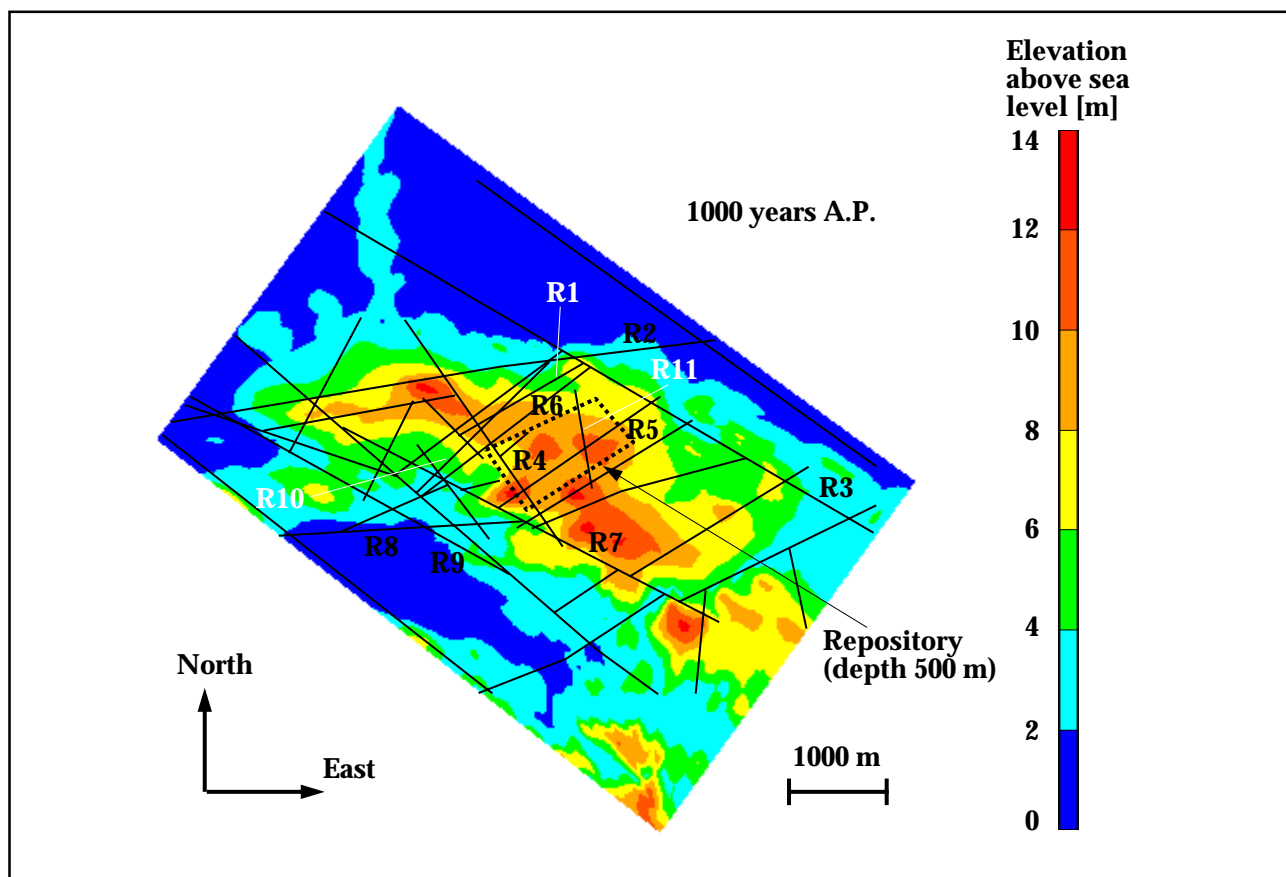
The simulation of the drilled well #3 showed

Figure 3b. *Surface boundary condition of the model at 1000 years after the present (A.P.).*

that flow routes may pass a shallow well unless it is located in the immediate vicinity of a discharge area. Therefore the shallow wells #4 – #6 above the bedrock were placed near the discharge areas.

In the simulations of the shallow wells a conducting surface layer as deep as the well is employed in the model. Thus, in the cases of the wells #5 and #6 the conducting layer is 5 metres deep and 10 metres in the case of the well #4. The fracture zones are not included in the conducting layer. Thus, the well #4 is located at the top of the fracture zone R3, the well #5 in the intersection of the fracture zones R8 and R9 and the well #6 at the top of the zone R2. The hydraulic conductivity of the surface layer is about $1.0 \cdot 10^{-5}$ m/s giving an infiltration approximately 30 % of the precipitation in the cases of the wells #5 and #6 and about 40 % of the precipitation in the case of the well #4. The infiltration was calculated at the depth of 2.5 metres, which is the depth of the centre of the uppermost element layer. The shallow wells are modelled by giving a residual pressure boundary condition p_r=0 Pa in the node depicting the well at the bottom of the conducting layer.

The wells #4 and #5 are modelled only at the last time step at 1000 years A.P., because the vicinity of the 1000 years A.P. discharge areas (SB1 and SB2 in Fig. 4) is still under the sea at 100 years A.P. The well #6 is modelled from 100 years A.P. on.
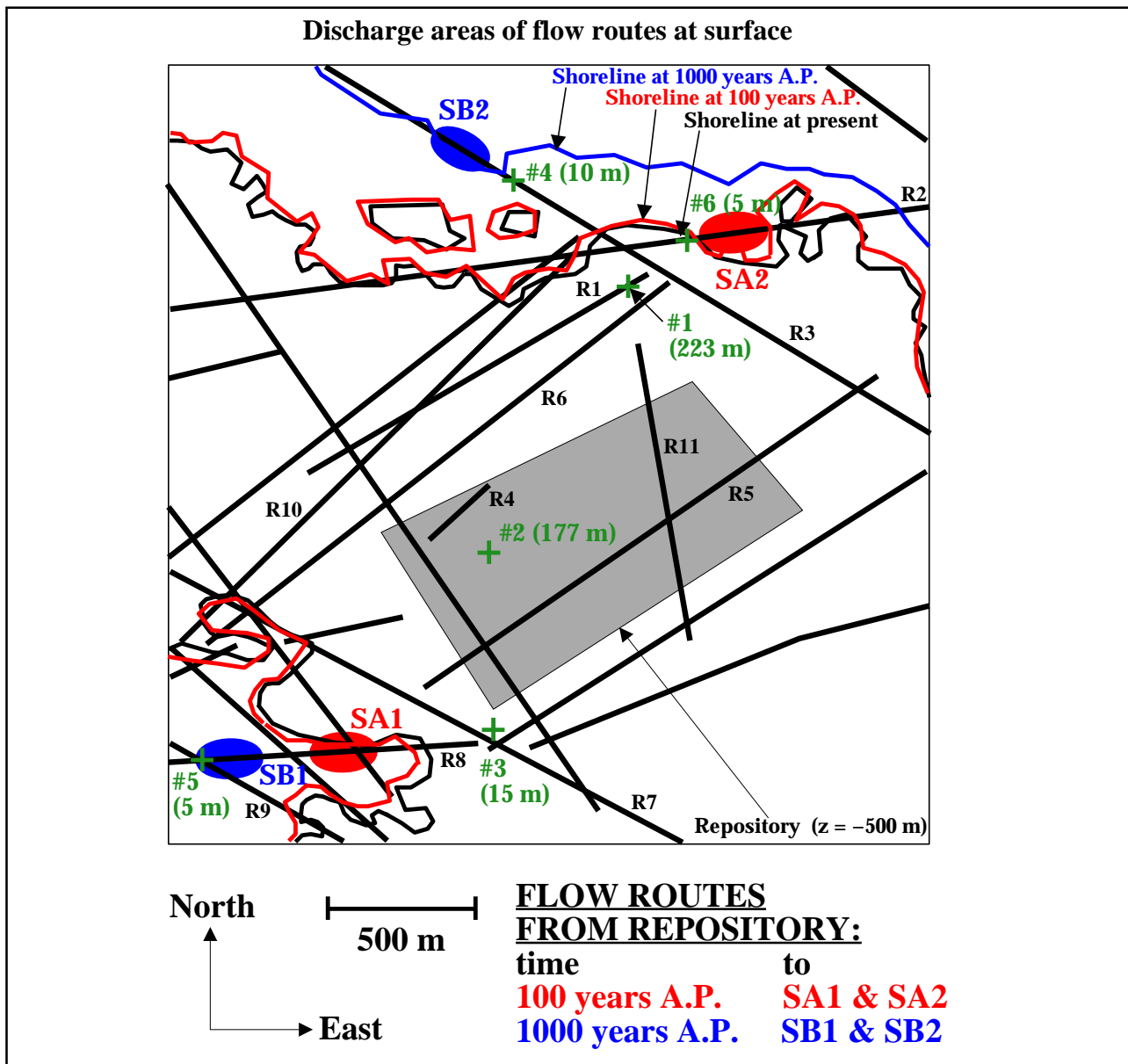

Figure 4. *Wells and discharge areas of flow routes. The gray quadrangular region presents the repository at the depth of 500 metres.*

4 RESULTS

4.1 General

Figure 5 shows how the wells #1, #2 and #5 (see Fig. 4) modify the pressure field. The figure presents the difference between the residual pressure fields in the cases without the well and with it. The cases of the wells #1 and #2 show that the influence of a drilled well may extend deep in the model. A drilled well may modify the pressure field even at the repository depth. The largest influences occur in the very vicinity of the well, however. Therefore, near the discharge areas even a shallow well may remarkably redirect the flow routes thus entering the well. This can be seen in the case of the well #5, which is located in the discharge area.

The flow routes from the repository were also calculated with a homogeneous model with the hydraulic conductivity $K=5.0 \cdot 10^{-9}$ m/s throughout the model (Figure 6). Due to the larger Darcy velocities deep in the model compared to the actual case, tenfold flow porosities were used to justify the boundary condition on the vertical edges. Next the hydraulic conductivity K was given the depth dependency (Eqs. (10) and (11)). The decrease in the Darcy velocities results in the flow routes moving upper and even discharging in the model area (Figure 7). However, no flow routes were entering the well #1, which was considered in these cases. In the cases shown in Figures 6 and 7 the flow routes seem to distribute more homogeneously than in the actual case of computation (Figure 8). Figure 8 shows how the structures channel the flow. This indicates a higher dilution in the well in the homogeneous and the only depth dependent cases compared to the actual case of computation.

4.2 Approaches

The effective dilution volume presents the volume of water in which the annual releases from the repository into the biosphere should be diluted to give the annual capacity of the well. It is thus the whole water volume within which the radionuclides from the repository are assumed to be diluted.

Three different approaches were used in the estimation of the dilution. The approaches A and B involve the flow route calculations. The approach C is based on the transport of a tracer.

The well capacity (m³/a), included in the approaches A and B, was calculated by surrounding the nodes describing the well with a control volume. The area of the horizontal cross-section of the control volume was 1 m². The volume extended from the surface to 0.25 m deeper than the lowermost well node.

The flow routes from the repository were determined from the continuous Darcy velocity field. The flow route analysis was performed at 100 and 1000 years A.P. assuming fixed hydraulic conditions at these time instants. The outcome of this flow route analysis should not be considered as real path lines, but "snapshots" in time with fixed flow and salinity field. However, it demonstrates the potential flow routes and the effect of the evolving hydraulic conditions on the routes and the discharge areas.

The total flow rate from the repository (m³/a), needed in the approaches B and C, was calculated by surrounding the two-dimensional plate describing the repository with a control volume. The height of the control volume was 50 metres.

4.2.1 Approach A

In the first approach 1500 flow routes were calculated from the repository. The starting points in the plate describing the repository were distributed uniformly excluding the fracture zones R10 and R11, which intersect the repository plate. The effective dilution volume in this approach is defined as

$$\frac{\text{well capacity } (\text{m}^3/\text{a})}{(\frac{n_{\text{well routes}}}{n_{\text{total}}})} \quad , \tag{18}$$
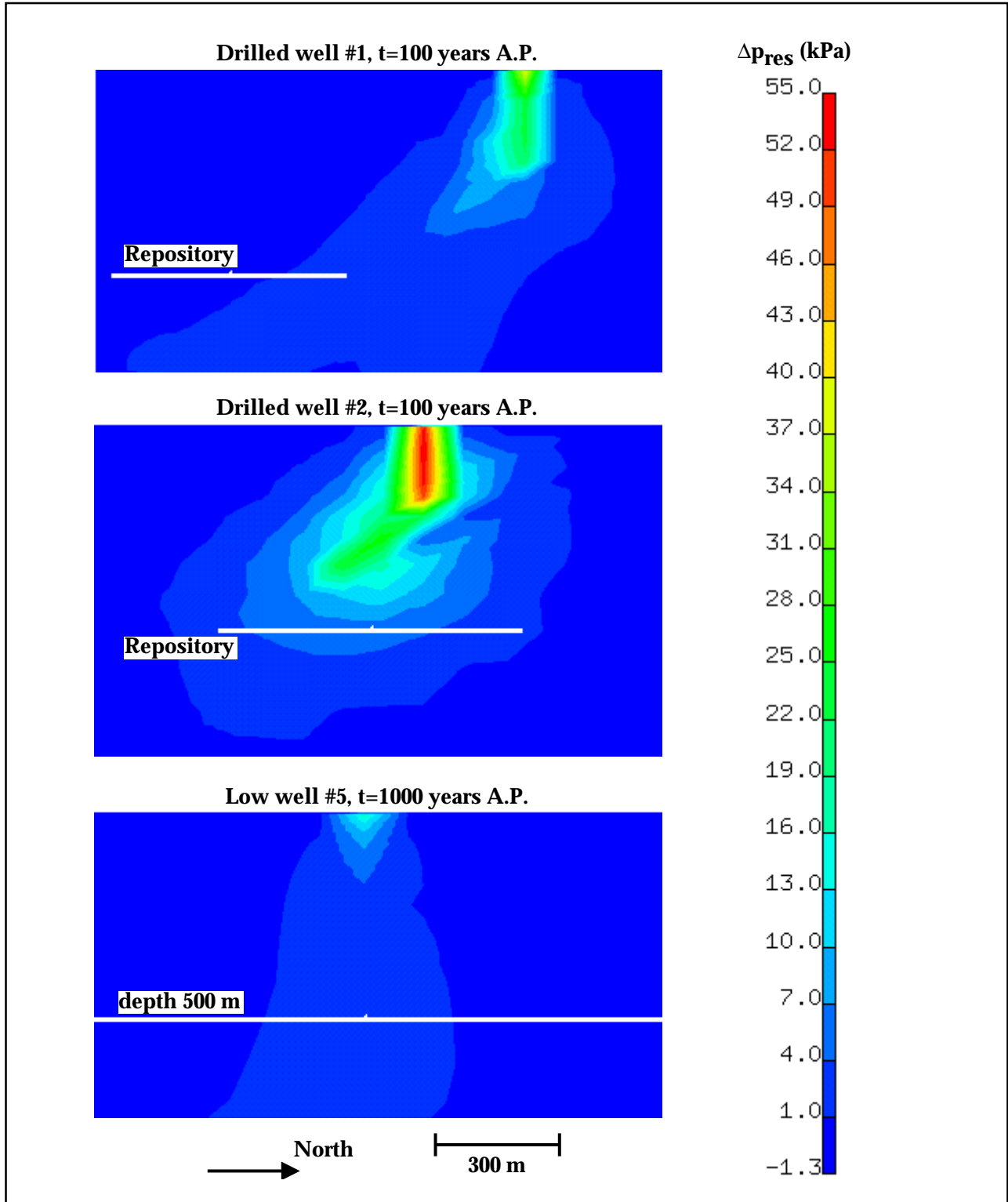

Figure 5. *Influence of wells #1, #2 and #5 on the pressure field.*

where $n_{\text{well routes}}$ is the number of flow routes entering the well and n_{total} is the total number of flow routes from the repository.

The fraction in the denominator of the expression (18) describes the portion of water flowing through the repository and entering the well. Thus, the flow routes starting from canisters are associated with equal fluxes. Figure 8 presents the characteristics of the approach A in the case of the well #1.
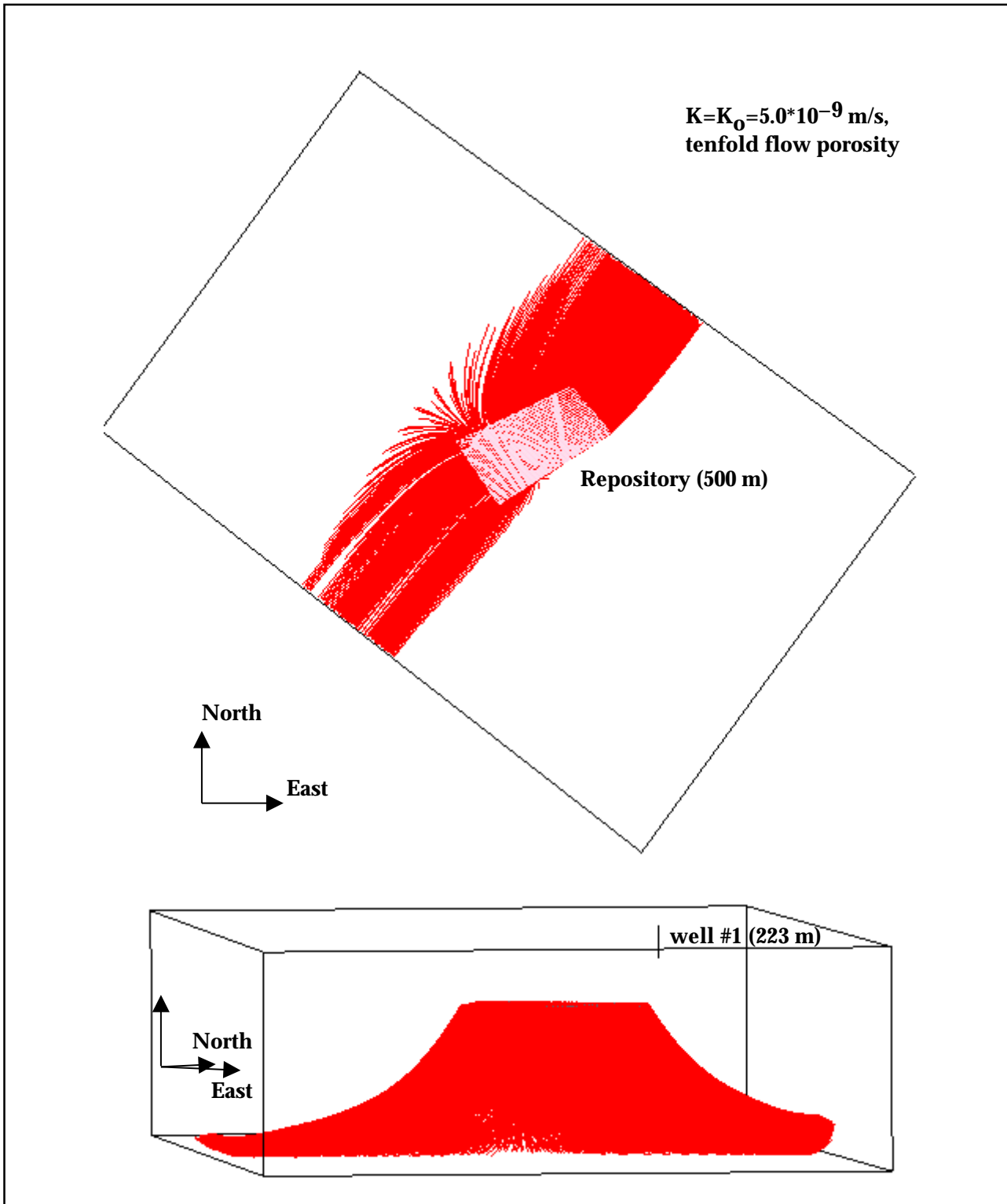

K=K$_0$=5.0*10^{-9} m/s, tenfold flow porosity

Repository (500 m)

North

East

well #1 (223 m)

North

East

Figure 6. *Flow routes from repository in the homogeneous model.*

4.2.2 Approach B

In the second approach the starting points of the flow routes were distributed uniformly in the plate describing the repository. The effective dilution volume in this approach is defined as

$$\frac{\text{well capacity (m}^3/\text{a})}{(\dfrac{\sum_i Q_{\text{well route } i}}{Q_{\text{repository}}})} \quad , \tag{19}$$

where $Q_{\text{well route } i}$ is the flow rate (m³/a) associated with the flow route i entering the well and $Q_{\text{repository}}$

$$K = K_O * 10^{f(z)},$$
where $K_O = 5.0*10^{-9}$ m/s
and
$$f(z) = 7*10^{-10}*z^3 + 3*10^{-6}*z^2 + 5*10^{-3}*z$$

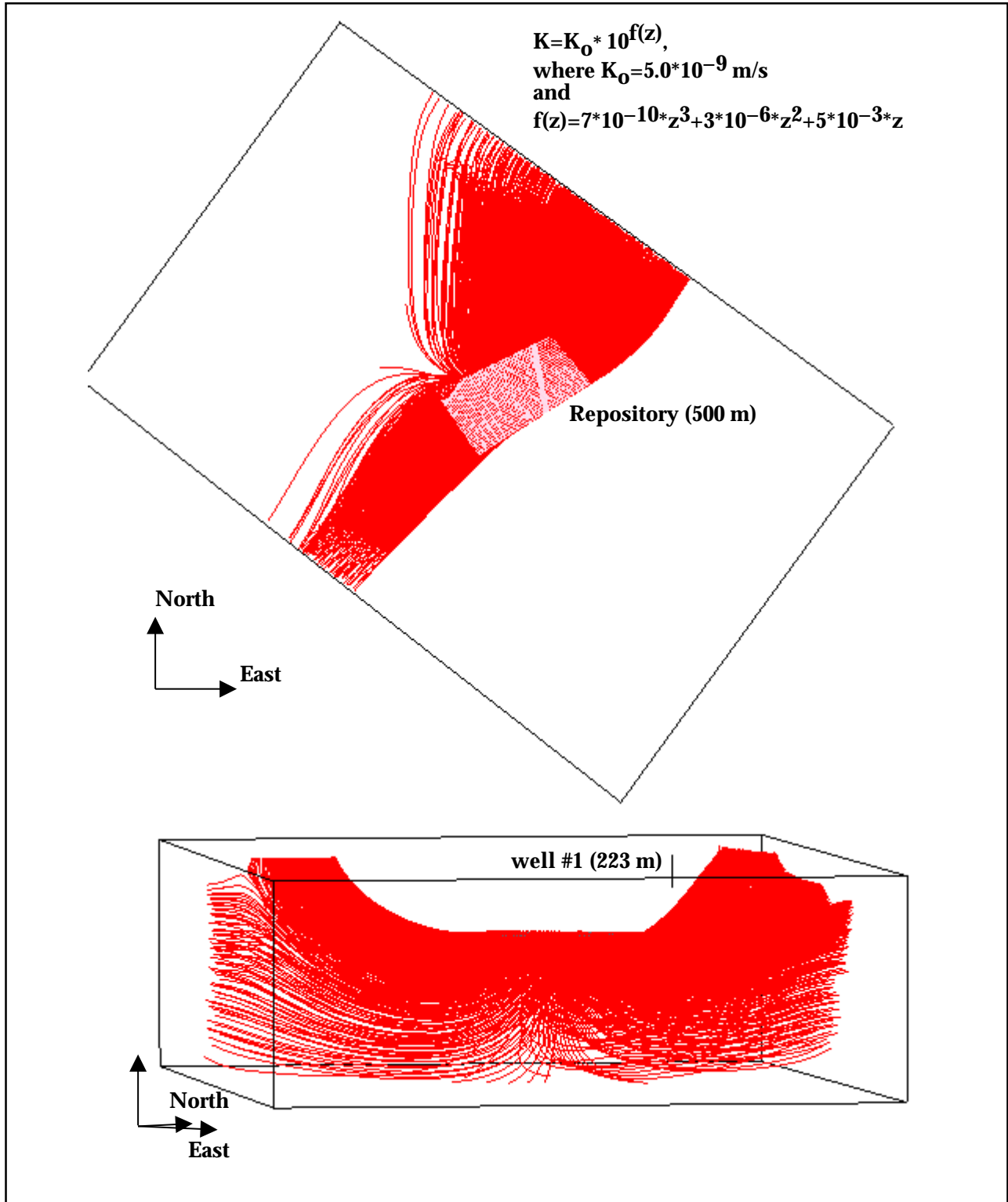Repository (500 m)

North

East

well #1 (223 m)

North

East

Figure 7. *Flow routes from repository in the model with depth dependent hydraulic conductivity.*

is the total flow rate from the repository (m³/a).

First, the repository plate was divided in elements, in which the flow rates were calculated. The starting points of the flow routes were then set in the center points of the elements. Thus, each flow route could be associated with the flow rate of an element.

The summed up flow rate, pertaining to the flow routes entering the well, divided by the total flow rate through the repository describes the portion of water flowing through the repository and entering the well. Due to this effort to take
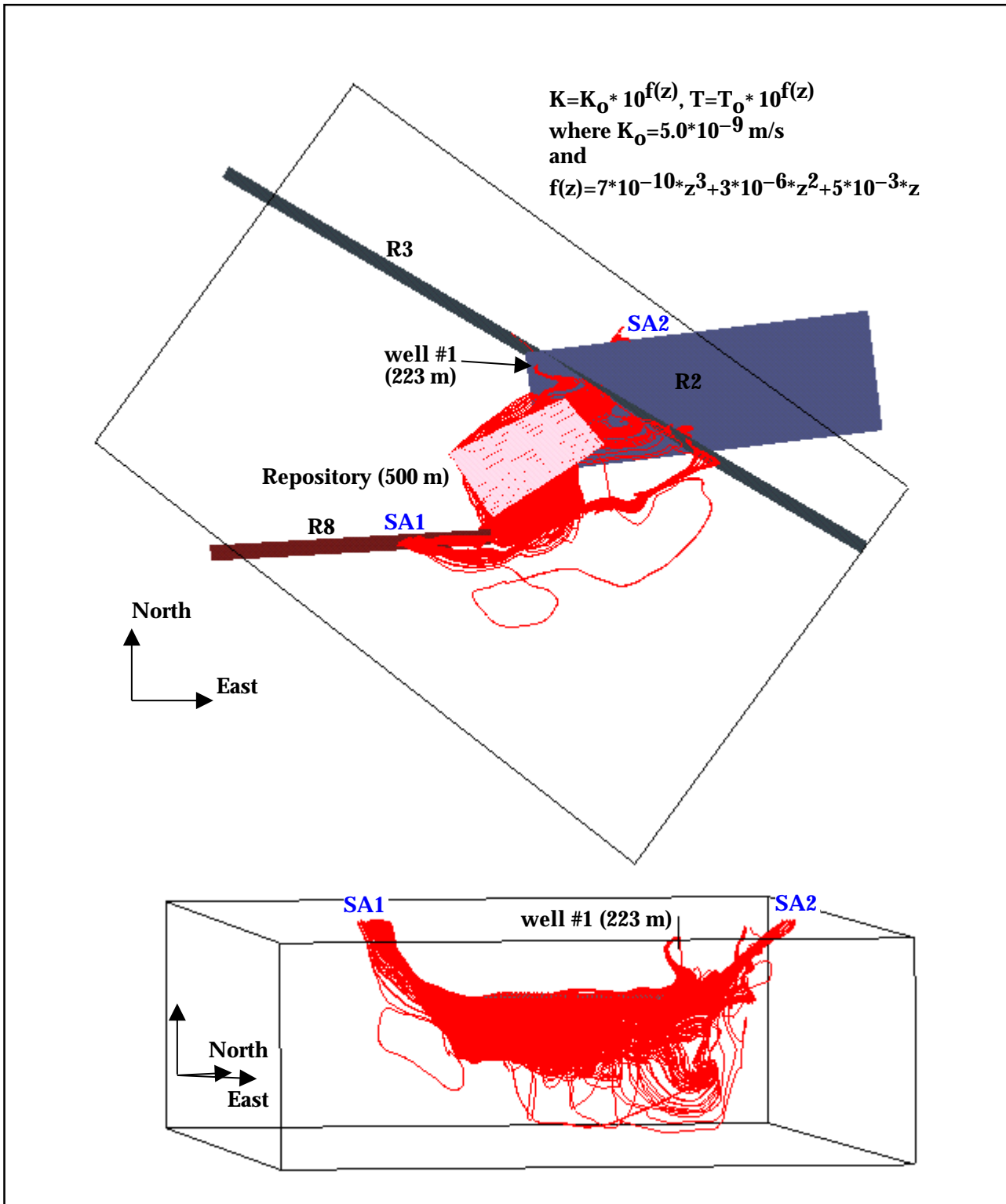

$K = K_0 * 10^{f(z)}$, $T = T_0 * 10^{f(z)}$
where $K_0 = 5.0 * 10^{-9}$ m/s
and
$f(z) = 7*10^{-10}*z^3 + 3*10^{-6}*z^2 + 5*10^{-3}*z$

Figure 8. *Flow routes from the repository in the case of the drilled well #1.*

into account the varying flux in the repository this approach could be considered as the most realistic approach used in this work.

4.2.3 Approach C

The third approach involves the transport calculation based on the simulated residual pressure and salinity fields. Initially, the tracer is defined to exist only in the repository. Zero concentration is used on the model edges and in the interior nodes excluding the repository nodes. In the first time step the initial boundary condition in the interior nodes is released—also in the repository nodes. Thus, the concentration of the tracer can decrease in the repository as function of time. The effective dilution volume in this approach is defined as

$$\frac{C_{\text{repository}}}{\overline{C}_{\text{well}}} \cdot Q_{\text{repository}}, \qquad (20)$$

where $C_{\text{repository}}$ is the concentration (kg/m³) in the repository and $\overline{C}_{\text{well}}$ is the mean concentration in the well (kg/m³). High uncertainty is associated with the surface boundary condition, which would largely determine the concentration in the shallow wells. Therefore, this approach was used only in the cases of the drilled wells #1 and #2.

4.3 Dilution volume

The main results are presented in the following three tables at 100 years and 1000 years A.P. Table III presents the well capasities (m³/a). Table IV summarizes the flow rates (m³/a) from the repository. The essential estimates of the effective dilution volume (m³/a) from the three approaches A, B and C are shown in Table V.

The capacity of the drilled well #2 at 100 years A.P. is perhaps too small to be used as a source of water, only 440 m³/a (Table III). The corresponding cells in Tables III–V are **black**. At 1000 years A.P. the capacity of the well #2 is somewhat larger. However, the capacities of the wells #2 and #4 at 1000 years are the lowest considered—less than 700 m³/a.

The wells #4 and #5 are modelled only at the last time step at 1000 years A.P., because their location is still under the sea at 100 years A.P. (Fig. 4). The corresponding cells in Tables III–V are also black.

The symbol infinite ∞ in Table V indicates that no flow routes were entering the well in that case. As previously mentioned, the approach C was used only in the cases of the drilled wells #1 and #2.

Overall, the wells were chosen so that a finite dilution volume would result. Thus, a randomly chosen well would more probably result in an infinite dilution volume. Looking at Figure 8 one can see how the channelling of the flow routes is critical for the dilution result of a well. A deep well may extend to the area of the deep flow routes, but in order to get flow routes into a shallow well, it has to be placed in the immediate vicinity of the discharge areas.

Near the discharge areas even a shallow well may remarkably redirect the nearby flow routes. Thus, the dilution calculated in a shallow well may be nearly equal to that calculated in a deep well. For instance, the estimates of the dilution volume in the approach A both for the drilled wells #1 and #2 and the shallow well #5 are from 29 000 m³/a to 64 000 m³/a, which do not differ very much.

The smallest estimate for the dilution volume is about 29 000 m³/a in the case of the shallow well #5 (Table V). Overall, the estimates for the dilution volume are the smallest in the approach A and the largest in the approach C, as far as there are flow routes entering the wells. Also, if there are flow routes, the estimates at 1000 years A.P. are smaller than at 100 years A.P. The largest variation in the finite estimations between the wells and time instants occurs in the approach B, about 250 000 m³/a. In the approach A the variation is the lowest, about 35 000 m³/a.

The approach B allows the consideration of the heterogeneity of the flow regime. Therefore, this approach may describe the dilution of activity most realistically in this work. The approach C integrates the transport of the tracer into the flow field simulation. However, the dispersion in the model causes uncertainty in the tracer transport calculations.

Significant uncertainty is known to relate to the estimates of the dilution volume. Therefore, two sensitivity cases were considered concerning the dilution in the drilled well #1 and the shallow well #5. The transmissivities of the major fracture zones pertaining to the flow into the wells were increased fivefold. Thus, in the case of the well #1

Table III. *Well capacities (m³/a).*

well (d (m))	100 years A.P.	1000 years A.P.
#1 (223 m)	10 700	23 700
#2 (177 m)	440	690
#3 (15 m)	9 200	22 900
#4 (10 m)		660
#5 (5 m)		1 950
#6 (5 m)	760	2 200

Table IV. *Flow rate from repository (m³/a).*

well (d (m))	100 years A.P.	1000 years A.P.
#1 (223 m)	55	58
#2 (177 m)	48	45
#3 (15 m)	53	52
#4 (10 m)	53	51
#5 (5 m)	53	51
#6 (5 m)	53	52

Table V. *Effective dilution volume (m³/a).*

well (d (m))	100 years A.P.			1000 years A.P.		
	A	B	C	A	B	C
#1 (223 m)	59 000	121 000	479 000	35 000		427 000
#2 (177 m)	∞	∞	**619 000**	64 000	311 000	458 000
#3 (15 m)		∞	—		∞	—
#4 (10 m)					∞	—
#5 (5 m)				29 000	122 000	—
#6 (5 m)		∞	—		∞	—

Table VI. *Effective dilution volumes (m³/a) in the sensitivity cases, in which the transmissivities of the major fracture zones pertaining to the flow into the wells were increased fivefold.*

well (d (m))	100 years A.P.			1000 years A.P.		
	A	B	C	A	B	C
#1 (223 m)	71 000	76 000	810 000	108 000	166 000	1 690 000
#5 (5 m)				66 000	154 000	—

the transmissivities of the zones R1 and R11 were $5 \cdot 10^{-5}$ m²/s and the transmissivity of the zone R2 was $2.2 \cdot 10^{-3}$ m²/s (see Fig. 4). In the case of the well #5 the transmissivities of the zones R7, R8 and R9 were $2.2 \cdot 10^{-3}$ m²/s each.

The sensitivity cases showed that an increasing portion of the water flowing through the repository enters the wells. Concurrently, the well capacities increase, however. These together result in larger effective dilution volumes than in the actual results except for the estimation pertaining to the approach B and the well #1 at 100 years A.P. (Table VI). In the sensitivity cases considered the estimates of the dilution volume based on the flow path calculations are in the range of variation of the actual estimates given in Table V. The estimates based on the transport calculations are even larger than the actual results. In any case, due to the powerful modification of the transmissivities the dilution volumes change tens of thousands of cubic metres per year.

4.4 Dose estimates

This report focuses only on the evaluation of doses related to the drinking water pathway, which is generally regarded to be one of the most important exposure routes and a simply defined reference case.

According to the groundwater flow analyses the uncentainty bound related to the effective dilution volume of the well seems to be about an order of magnitude: from 30 000 m³/a to 460 000 m³/a. In conservative considerations the value of 90 000 m³/a could be regarded as a representative expectation value of the effective dilution of the well. This dilution volume value was also suggested by the most realistic modelling approach of the groundwater flow analysis. It has been used as a base value when calculating nuclide specific dose conversion factors (DCF's) for the drinking water pathway; the values presented in Table VII. The DCF's in Table VII were calculated for unit re-

Table VIIa. *Dose conversion factors (DCF's) of fission and activation products for the well water drinking pathway.*

Nuclide	Half-life (year)	Ingestion dose coefficient (Sv/Bq)	Expected[1] DCF (Sv/Bq)
C-14	$5.7 \cdot 10^3$	$5.8 \cdot 10^{-10}$	$\mathbf{4.7 \cdot 10^{-15}}$
Cl-36	$3.0 \cdot 10^5$	$9.3 \cdot 10^{-10}$	$\mathbf{7.5 \cdot 10^{-15}}$
Ni-59	$7.5 \cdot 10^4$	$6.3 \cdot 10^{-11}$	$\mathbf{5.1 \cdot 10^{-16}}$
Se-79	$6.4 \cdot 10^4$	$2.9 \cdot 10^{-9}$	$\mathbf{2.4 \cdot 10^{-14}}$
Sr-90 + d			$\mathbf{2.5 \cdot 10^{-13}}$
Sr-90	$2.9 \cdot 10^1$	$2.8 \cdot 10^{-8}$	$2.3 \cdot 10^{-13}$
Y-90	$7.3 \cdot 10^{-3}$	$2.7 \cdot 10^{-9}$	$2.2 \cdot 10^{-14}$
Zr-93 + d			$\mathbf{9.9 \cdot 10^{-15}}$
Zr-93	$1.5 \cdot 10^6$	$1.1 \cdot 10^{-9}$	$8.9 \cdot 10^{-15}$
Nb-93m	$1.4 \cdot 10^1$	$1.2 \cdot 10^{-10}$	$9.7 \cdot 10^{-16}$
Nb-94	$2.0 \cdot 10^4$	$1.7 \cdot 10^{-9}$	$\mathbf{1.4 \cdot 10^{-14}}$
Tc-99	$2.1 \cdot 10^5$	$6.4 \cdot 10^{-10}$	$\mathbf{5.2 \cdot 10^{-15}}$
Pd-107	$6.5 \cdot 10^6$	$3.7 \cdot 10^{-11}$	$\mathbf{3.0 \cdot 10^{-16}}$
Sn-126 + d			$\mathbf{5.7 \cdot 10^{-14}}$
Sn-126	$1.0 \cdot 10^5$	$4.7 \cdot 10^{-9}$	$3.8 \cdot 10^{-14}$
Sb-126[2]	$3.4 \cdot 10^{-2}$	$2.4 \cdot 10^{-9}$	$1.9 \cdot 10^{-14}$
I-129	$1.6 \cdot 10^7$	$1.1 \cdot 10^{-7}$	$\mathbf{8.9 \cdot 10^{-13}}$
Cs-135	$2.3 \cdot 10^6$	$2.0 \cdot 10^{-9}$	$\mathbf{1.6 \cdot 10^{-14}}$
Cs-137	$3.0 \cdot 10^1$	$1.3 \cdot 10^{-8}$	$\mathbf{1.1 \cdot 10^{-13}}$

1) Effective dilution volume of well used is **90 000 m³/a**. Water consumption rate assumed is 2 litres/day.

2) The intensity of the Sn-126 → Sb-126m→ Sb-126 decay is 14% (Kocher, 1981).

Table VIIb. *Dose conversion factors (DCF's) of 4N and 4N+1 chains nuclides for the well water drinking pathway.*

Nuclide	Half-life (year)	Ingestion dose coefficient (Sv/Bq)	Expected[1] DCF (Sv/Bq)
Pu-240	$6.5 \cdot 10^3$	$2.5 \cdot 10^{-7}$	$\mathbf{2.0 \cdot 10^{-12}}$
U-236	$2.3 \cdot 10^7$	$4.7 \cdot 10^{-8}$	$\mathbf{3.8 \cdot 10^{-13}}$
Th-232 + d			$\mathbf{8.6 \cdot 10^{-12}}$
Th-232	$1.4 \cdot 10^{10}$	$2.3 \cdot 10^{-7}$	$1.9 \cdot 10^{-12}$
Ra-228	$5.8 \cdot 10^0$	$6.9 \cdot 10^{-7}$	$5.6 \cdot 10^{-12}$
Th-228	$1.9 \cdot 10^0$	$7.2 \cdot 10^{-8}$	$5.8 \cdot 10^{-13}$
Ra-224	$1.0 \cdot 10^{-2}$	$6.5 \cdot 10^{-8}$	$5.3 \cdot 10^{-13}$
Cm-245 + d			$\mathbf{1.7 \cdot 10^{-12}}$
Cm-245	$8.5 \cdot 10^3$	$2.1 \cdot 10^{-7}$	$1.7 \cdot 10^{-12}$
Pu-241	$1.4 \cdot 10^1$	$4.8 \cdot 10^{-9}$	$3.9 \cdot 10^{-14}$
Am-241	$4.3 \cdot 10^2$	$2.0 \cdot 10^{-7}$	$\mathbf{1.6 \cdot 10^{-12}}$
Np-237 + d			$\mathbf{9.0 \cdot 10^{-13}}$
Np-237	$2.1 \cdot 10^6$	$1.1 \cdot 10^{-7}$	$8.9 \cdot 10^{-13}$
Pa-233	$7.4 \cdot 10^{-2}$	$8.7 \cdot 10^{-10}$	$7.1 \cdot 10^{-15}$
U-233	$1.6 \cdot 10^5$	$5.1 \cdot 10^{-8}$	$\mathbf{4.1 \cdot 10^{-13}}$
Th-229 + d			$\mathbf{5.0 \cdot 10^{-12}}$
Th-229	$7.3 \cdot 10^3$	$4.9 \cdot 10^{-7}$	$4.0 \cdot 10^{-12}$
Ra-225	$4.1 \cdot 10^{-2}$	$9.9 \cdot 10^{-8}$	$8.0 \cdot 10^{-13}$
Ac-225	$2.7 \cdot 10^{-2}$	$2.4 \cdot 10^{-8}$	$1.9 \cdot 10^{-13}$

1) Effective dilution volume of well used is **90 000 m³/a**. Water consumption rate assumed is 2 litres/day.

lease rates (1 Bq/a) and the assumed water consumption rate was 2 litres/day.

The value of a nuclide specific DCF (Sv/Bq) is simply obtained as follows:

$$DCF_i = \frac{\dot{H}_i}{Q_i} = \frac{I_w \cdot d_{ing,i}}{F_{eff}}, \qquad (21)$$

where

I_w is the consumption rate of water (m³/a),
$d_{ing,i}$ is the ingestion dose coefficient (Sv/Bq),
F_{eff} is the effective dilution volume (m³/a),
Q_i is the total release rate into the rock volume affected by the well (Bq/a) and
$\dot{H}_i$ is the individual dose rate (Sv/a).

The ingestion dose coefficients applied in this report are based on the ICRP Publication 72 recommendations (ICRP, 1996).

As an illustrative example dose responses from a release scenario of spent fuel disposal in Finnish bedrock have been considered. The leakage from the disposal canister and subsequent release of radionuclides to the biosphere is assumed to be caused by a small hole in a defected disposal canister (Vieno & Nordman, 1999). The release rates of this safety case have been applied to the DCF's from Table VII. Annual individual doses via the drinking water pathway for the most important nuclides are presented in Fig. 9. The most

Table VIIc. *Dose conversion factors (DCF's) of 4N+2 chain nuclides for the well water drinking pathway.*

Nuclide	Half-life (year)	Ingestion dose coefficient (Sv/Bq)	Expected[1] DCF (Sv/Bq)
Cm-246	$4.7 \cdot 10^3$	$2.1 \cdot 10^{-7}$	**$1.7 \cdot 10^{-12}$**
Pu-242	$3.8 \cdot 10^5$	$2.4 \cdot 10^{-7}$	**$1.9 \cdot 10^{-12}$**
U-238 + d			**$4.0 \cdot 10^{-13}$**
U-238	$4.5 \cdot 10^9$	$4.5 \cdot 10^{-8}$	$3.7 \cdot 10^{-13}$
Th-234	$6.6 \cdot 10^{-2}$	$3.4 \cdot 10^{-9}$	$2.8 \cdot 10^{-14}$
Pu-238	$8.8 \cdot 10^1$	$2.3 \cdot 10^{-7}$	**$1.9 \cdot 10^{-12}$**
U-234	$2.5 \cdot 10^5$	$4.9 \cdot 10^{-8}$	**$4.0 \cdot 10^{-13}$**
Th-230	$7.7 \cdot 10^4$	$2.1 \cdot 10^{-7}$	**$1.7 \cdot 10^{-12}$**
Ra-226 + d			**$1.8 \cdot 10^{-11}$**
Ra-226	$1.6 \cdot 10^3$	$2.8 \cdot 10^{-7}$	$2.3 \cdot 10^{-12}$
Rn-222	$1.0 \cdot 10^{-2}$	$1 \cdot 10^{-8}$	$8.1 \cdot 10^{-14}$
Pb-210	$2.2 \cdot 10^1$	$6.9 \cdot 10^{-7}$	$5.6 \cdot 10^{-12}$
Bi-210	$1.4 \cdot 10^{-2}$	$1.3 \cdot 10^{-9}$	$1.1 \cdot 10^{-14}$
Po-210	$3.8 \cdot 10^{-1}$	$1.2 \cdot 10^{-6}$	$9.7 \cdot 10^{-12}$

1) Effective dilution volume of well used is **90 000 m³/a**. Water consumption rate assumed is 2 litres/day.

Table VIId. *Dose conversion factors (DCF's) of 4N+3 chain nuclides for the well water drinking pathway.*

Nuclide	Half-life (year)	Ingestion dose coefficient (Sv/Bq)	Expected[1] DCF (Sv/Bq)
Am-243 + d			**$1.6 \cdot 10^{-12}$**
Am-243	$7.4 \cdot 10^3$	$2.0 \cdot 10^{-7}$	$1.6 \cdot 10^{-12}$
Np-239	$6.5 \cdot 10^{-3}$	$8.0 \cdot 10^{-10}$	$6.5 \cdot 10^{-15}$
Pu-239	$2.4 \cdot 10^4$	$2.5 \cdot 10^{-7}$	**$2.0 \cdot 10^{-12}$**
U-235 + d			**$3.8 \cdot 10^{-13}$**
U-235	$7.0 \cdot 10^8$	$4.7 \cdot 10^{-8}$	$3.8 \cdot 10^{-13}$
Th-231	$2.9 \cdot 10^{-3}$	$3.4 \cdot 10^{-10}$	$2.8 \cdot 10^{-15}$
Pa-231 + d			**$1.6 \cdot 10^{-11}$**
Pa-231	$3.3 \cdot 10^4$	$7.1 \cdot 10^{-7}$	$5.8 \cdot 10^{-12}$
Ac-227	$2.2 \cdot 10^1$	$1.1 \cdot 10^{-6}$	$8.9 \cdot 10^{-12}$
Th-227	$5.1 \cdot 10^{-2}$	$8.8 \cdot 10^{-9}$	$7.1 \cdot 10^{-14}$
Ra-223	$3.1 \cdot 10^{-2}$	$1.0 \cdot 10^{-7}$	$8.1 \cdot 10^{-13}$

1) Effective dilution volume of well used is **90 000 m³/a**. Water consumption rate assumed is 2 litres/day.

important nuclides are I-129, Cs-135 and C-14; I-129 dominating the doses for the whole release period.

The recent ICRP Publication 81 suggests an individual annual dose constraint of 0.3 mSv for the spent fuel disposal (ICRP, 2000). According to the present understanding and modelling capability related to the safety analyses of spent fuel disposal, the future doses arising from spent fuel disposal are several orders of magnitude below the internationally accepted dose constraints (see Fig. 9).
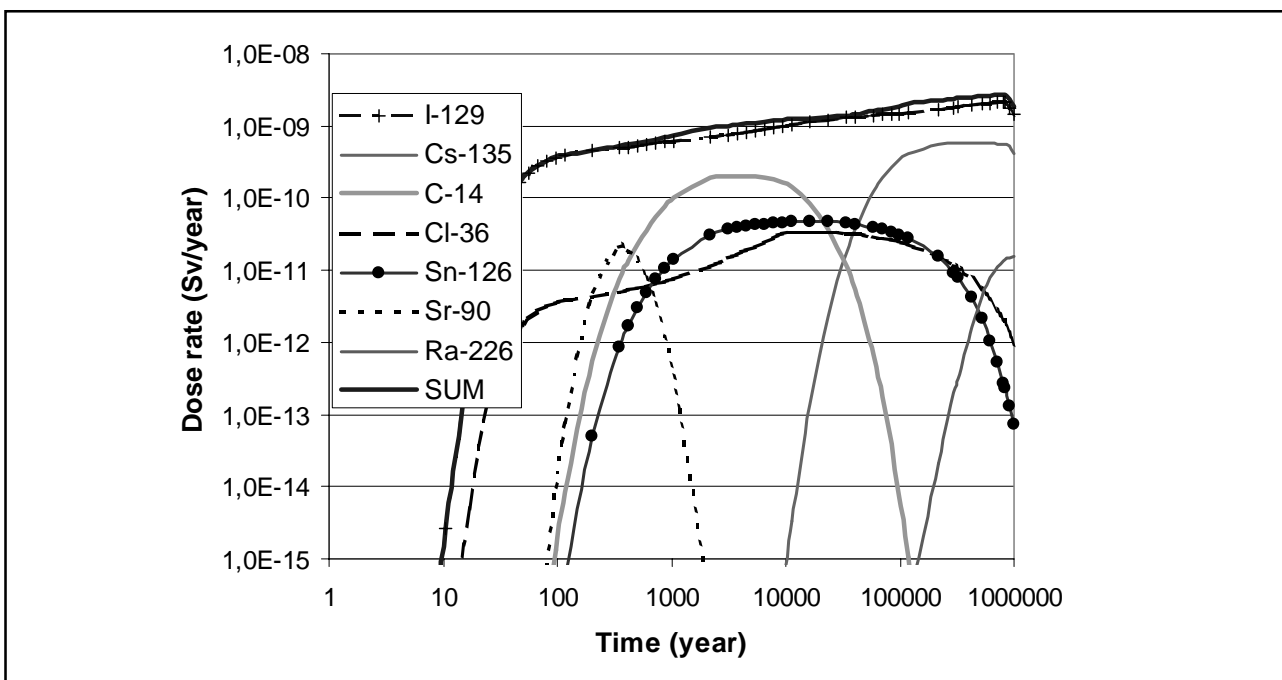

Figure 9. *Dose rates of the most important nuclides of the well water drinking pathway.*

5 SUMMARY AND CONCLUSIONS

An estimate of the dilution volume should be based on a careful analysis of the results from a realistic groundwater flow and transport model. As regards to the placing and the depth of the wells several alternatives should be considered.

In the groundwater flow modelling part of this work the effective dilution volume in the well scenario was estimated by means of transient simulations of groundwater flow and transport, which are coupled due to the varying salinity. The task was performed by applying a model based on the porous medium concept and the finite element method. Both deep, drilled wells and shallow surface wells in the vicinity of the repository were considered. The simulations covered the time period from the present to 1000 years after the present.

Conceptually the fractured bedrock consists of planar fracture zones (with a high fracture density and a greater ability to conduct water) and the intact rock (in which the fracture density and the hydraulic conductivity are low). For them the equivalent-continuum model was applied separately. Thus, the fractured bedrock was considered as piecewise homogeneous (except for the depth dependence) and isotropic continuum with representative average characteristics. The repository and the surrounding disturbed zone of the bedrock were modelled as a planar structure. The modelled bedrock volume was assumed to be fully saturated.

A generic simulation model for groundwater flow and solute transport was developed on the basis of geological, hydrogeological and hydrogeochemical data at a coastal area. The simulation model contains all the data necessary for the numerical simulations, i.e. the groundwater table and topography, salinity, the postglacial land uplift and sea level rise, the conceptual geometry of fracture zones, the hydraulic properties of the bedrock as well as the description of the modelling volume.

The model comprises an area of about 26 km². It covers an island and the surrounding sea. The depth of the modelled domain is 1.5 km. Due to the exponentially decreasing hydraulic conductivity of the intact rock and the transmissivity of the fracture zones, the flow deeper in the bedrock can be considered insignificant.

Residual pressure based on the elevation of the groundwater table was used as surface boundary condition. In the rest of the modelled volume the initial pressure was assumed to be hydrostatic. The values of residual pressure assigned to the nodes were calculated from the fixed salinity distribution. On the vertical faces time-dependent residual pressures and salinity concentrations were used.

The finite element code FEFTRA (formerly known as FEFLOW) was used in this work for the numerical solution.

The dilution was considered in six wells. They were located in the vicinity of the discharge areas or in the intermediate region. They were modelled by giving a residual pressure boundary condition p_r=0 Pa in the nodes depicting the well. The places for the three drilled wells were chosen so that the salinity will not be very high in the bottom parts of the wells. In the cases of the shallow wells the topmost layers of the model describe the soil. The hydraulic conductivity of the soil was adjusted to allow an adequate portion of water to infiltrate into the modelled volume.

The channelling along the flow routes was found to be critical for the resulting in a well. A deep well may extend near the area of the deep flow routes, but in order to get flow routes into a shallow well, it has to be placed in the immediate vicinity of the discharge areas.

Two of the selected approaches utilised flow

route calculations, whereas the third involved tracer transport calculations using the simulated pressure and salinity fields. In the first approach the flow routes starting from canisters were associated with equal fluxes. In the second approach each flow route was assigned with a flow rate allowing the consideration of the heterogeneity of the flow regime. This approach may describe the dilution of activity most realistically in this work. The third approach was used only in the cases of the drilled wells, because the surface boundary condition would have largely determined the concentration in the shallow wells.

In the sensitivity cases some transmissivity modifications were considered. The estimates of the dilution volume based on the flow path calculations were in the range of variation of the actual estimates. The estimates based on the transport calculation were even larger than the actual results.

This report focused only on the evaluation of doses related to the drinking water pathway, which is generally regarded to be one of the most important exposure routes and a simply defined reference case.

According to the groundwater flow analyses the effective dilution volume of the well seems to vary from 30 000 m^3/a to 460 000 m^3/a. Due to the placing of the shallow wells in the discharge areas, the dilution calculated in the shallow well was shown to be close to that calculated in the deep well. In case the location of the well is chosen randomly, in many cases no flow routes hit the volume affected by the well. In these cases the effective dilution volume would be infinite. In conservative considerations the value around 90 000 m^3/a can be regarded as a representative expectation value of the effective dilution of the well. This dilution volume value was also suggested by the most realistic modelling approach of the groundwater flow analysis. It was used as basis when calculating the nuclide specific dose conversion factors (DCF's) for the drinking water pathway. The DCF's were calculated for unit release rates (1 Bq/a) and the assumed water consumption rate was 2 litres/day.

REFERENCES

Anon., 1986. Applied Hydrology. Vesiyhdistys ry., Helsinki. (In Finnish).

Bear, J., 1979. Hydraulics of Groundwater. McGraw-Hill, Israel.

Brooks, A. N. & Hughes, T. J. R., 1992. Streamline Upwind/Petrov-Galerkin Formulations for Convection Dominated Flows with Particular Emphasis on the Incompressible Navier-Stokes Equations. Computer Methods in Applied Mechanics and Engineering, 32:199–259.

FEFTRA, 1999. Home Pages for FEFTRA in Internet. http://www.vtt.fi/ene/ye/feftra/index.html.

Huyakorn, P. S. & Pinder, G. F., 1983. Computational Methods in Subsurface Flow. Academic Press INC, Orlando.

ICRP, 1996. Age-dependent Doses to Members of the Public from Intake of Radionuclides: Part 5 Compilation of Ingestion and Inhalation Dose Coefficients. International Commission on Radiological Protection, ICRP Publication 72.

ICRP, 2000. Radiation Protection Recommendations as Applied to the Disposal of Long-lived Solid Radioactive Waste. ICRP Publication 81.

Kocher, D. C., 1981. Radioactive Decay Data Tables. U.S. Department of Energy, Technical Information Center, DOE/TIC-11026.

Laitinen, M., 1994. Developing an Iterative Solver for the FEFLOW Package. Technical Report POHJA-2/94, VTT Energy, Espoo. (In Finnish).

Laitinen, M., 1995. Modelling Convection Dominated Transport Problems with Improved Galerkin Finite Element Formulations. VTT Julkaisuja – Publikationer 804 VTT-JULK-804, Technical Research Centre of Finland, Espoo. (In Finnish).

Lampén, P. & Snellman, M., 1993. Summary Report on Groundwater Chemistry. Report YJT-93-14, Nuclear Waste Commission of Finnish Power Companies, Helsinki.

Lide, D. R. (ed.), 1990. CRC Handbook of Chemistry and Physics. 71st Edition 1990–1991. CRC Press, Inc., Boston.

Löfman, J. & Taivassalo, V., 1993. FEFLOW 1.10 —Solving of Coupled Equations for Flow, Heat and Solute Transport. Report YJT-93-30, Nuclear Waste Commission of Finnish Power Companies, Helsinki. (In Finnish).

Löfman, J., 1999. Site Scale Groundwater Flow in Olkiluoto. Report POSIVA 99-03, Posiva Oy, Helsinki.

de Marsily, G., 1986. Quantitative Hydrogeology— Groundwater Hydrology for Engineers. Academic Press INC, Orlando.

Pusch, R., 1990. Radionuclide Transport Paths in the Nearfield—A KBS-3 Concept Study. Technical Report 90-32, Swedish Nuclear Fuel and Waste Management Co. (SKB), Stockholm.

Påsse, T., 1996. A Mathematical Model of the Shorelevel Displacement in Fennoscandia. Technical Report 96-24, Swedish Nuclear Fuel and Waste Management Co. (SKB), Stockholm.

Riekkola, R., Saanio, T. & Salo, J.-P., 1996. Preliminary Site Specific Adaptations of the Repository for Spent Nuclear Fuel. Work Report TEKA-96-07, Posiva Oy, Helsinki. (In Finnish).

Saksa, P., Nummela, J. & Ahokas, H., 1996. Bedrock Model of Eurajoki Olkiluoto Site. Supplemented and Revised Conceptual Description in the Year 1996. Work Report PATU-96-46, Posiva Oy, Helsinki. (In Finnish).

SKB, 1999. SR 97—Main Report. Technical Report 99-06, Swedish Nuclear Fuel and Waste Management Co. (SKB), Stockholm.

Taivassalo, V., Koskinen, L. & Mészáros, F., 1991. Further Development of the FEFLOW Code for Transient Simulations. Work Report 91-14, Teollisuuden Voima Oy (TVO), Helsinki. (In Finnish).

Taivassalo, V. & Saarenheimo, A., 1991. Groundwater Flow Analysis for the VLJ Repository. Report YJT-91-10, Teollisuuden voima Oy (TVO), Helsinki.

Vieno, T., Hautojärvi, A., Koskinen, L. & Nordman, H., 1992. TVO-92 Safety Analysis of Spent Fuel Disposal. Report YJT-92-33E, Nuclear Waste Commission of Finnish Power Companies, Helsinki.

Vieno, T. & Nordman, H., 1999. Safety Assessment of Spent Fuel Disposal in Hästholmen, Kivetty, Olkiluoto and Romuvaara, TILA-99. POSIVA 99-07, Posiva Oy, Helsinki.